HHS Public Access

Author manuscript

Nat Neurosci. Author manuscript; available in PMC 2024 February 05.

Published in final edited form as:

Nat Neurosci. 2023 April ; 26(4): 570–578. doi:10.1038/s41593-023-01270-2.

Forty-hertz light stimulation does not entrain native gamma oscillations in Alzheimer's disease model mice

Marisol Soula[1], **Alejandro Martín-Ávila**[2,3], **Yiyao Zhang**[1], **Annika Dhingra**[1], **Noam Nitzan**[1], **Martin J. Sadowski**[4,5], **Wen-Biao Gan**[3], **György Buzsáki**[1,2,4]

[1]Neuroscience Institute, Langone Medical Center, New York University, New York, NY, USA.

[2]Department of Physiology and Neuroscience, Langone Medical Center, New York University, New York, NY, USA.

[3]Skirball Institute of Biomolecular Medicine, Langone Medical Center, New York University, New York, NY, USA.

[4]Department of Neurology and Psychiatry, Langone Medical Center, New York University, New York, NY, USA.

[5]Department of Biochemistry and Molecular Pharmacology, Langone Medical Center, New York University, New York, NY, USA.

Abstract

There is a demand for noninvasive methods to ameliorate disease. We investigated whether 40-Hz flickering light entrains gamma oscillations and suppresses amyloid-β in the brains of APP/PS1 and 5xFAD mouse models of Alzheimer's disease. We used multisite silicon probe recording in the visual cortex, entorhinal cortex or the hippocampus and found that 40-Hz flickering simulation did not engage native gamma oscillations in these regions. Additionally, spike responses in the hippocampus were weak, suggesting 40-Hz light does not effectively entrain deep structures. Mice avoided 40-Hz flickering light, associated with elevated cholinergic activity in the hippocampus. We found no reliable changes in plaque count or microglia morphology by either immunohistochemistry or in vivo two-photon imaging following 40-Hz stimulation, nor reduced levels of amyloid-β 40/42. Thus, visual flicker stimulation may not be a viable mechanism for modulating activity in deep structures.

Reprints and permissions information is available at www.nature.com/reprints.

Correspondence and requests for materials should be addressed to György Buzsáki. gyorgy.buzsaki@nyulangone.org.

Author contributions

M.S., M.J.S., W.-B.G. and G.B. designed the research. M.S., Y.Z. and A.M.-A. performed the research. M.S., A.D., Y.Z. and N.N. analyzed the data. G.B. and M.S. wrote the paper.

Competing interests

The authors declare no competing interests.

Additional information

Extended data is available for this paper at https://doi.org/10.1038/s41593-023-01270-2.

Supplementary information The online version contains supplementary material available at https://doi.org/10.1038/s41593-023-01270-2.

Peer review information *Nature Neuroscience* thanks the anonymous reviewers for their contribution to the peer review of this work.

Brain oscillations are altered in many psychiatric and neurological conditions[1]. Thus, there is a strong appeal for discovering noninvasive methods to attenuate or restore physiological network oscillations[2]. A potential application includes Alzheimer's disease (AD), a progressive neurodegenerative disorder, characterized by abnormal aggregation of the proteins amyloid-β (Aβ) and hyperphosphorylated tau. There are currently no broadly effective disease-modifying therapies available for AD, making noninvasive methods a viable option. Recent work suggested that 40-Hz sensory stimulation, but not lower frequencies, is a potential treatment in AD[3–8]. Light, sound stimulation or their combination reduced levels of Aβ isoform in a mouse model of AD, associated with morphological transformation of microglia in both neocortex and hippocampus[3–5]. Based on previously demonstrated correlations between elevated spiking activity and Aβ levels in the interstitial fluid of the brain[9], the authors hypothesized that 40-Hz stimulation entrains native gamma rhythms in brain-wide areas[3–5], and this, therefore, is a potential mechanism of its beneficial effect[10]. More recently, it has been suggested that the combination of light flickering with exercise may also improve cognitive function by reducing Aβ and tau levels[11]. Another recent study implied that flickering light at 30–50 Hz can prevent the delayed neurodegeneration of hippocampal pyramidal neurons in forebrain transient ischemia[12]. Furthermore, 40-Hz optogenetic stimulation of the medial septum in an AD mouse model elevated performance in a spatial memory task, although the impact of stimulation on brain pathology was not evaluated[13]. However, the suggestion that flickering light stimulation can entrain brain-wide gamma oscillations stands in contrast to previous findings demonstrating that neutral sensory stimuli do not effectively engage higher-order cortical structures, unless the stimulus presents relevance to the animal[14–16].

Given the great potential therapeutic implications of these reports for the treatment of patients with AD, we investigated the role of acute and chronic 40-Hz stimulation in several AD mouse models[17]. Our data indicate that 40-Hz flickering light does not reliably reduce Aβ load in the neocortex or hippocampus, potentially due to the large variability of AD pathology. When given the option, mice avoided 40-Hz flickering light stimulation over continuous light of the same intensity. Only a small fraction of hippocampal and entorhinal neurons responded to light stimulation but without affecting innate gamma oscillations. Thus, the hypothesized flicker light entrainment of native gamma oscillations is not a strong candidate mechanism for reliably affecting AD pathology.

Results

Immunohistochemical changes following 40-Hz stimulation

We first examined the effect of 1 h of 40-Hz light stimulation on Aβ load at different stages of AD pathology in four cohorts of APP/PS1 and one cohort of 5xFAD mice (Fig. 1, Extended Data Fig. 1 and Supplementary Table 1). Control mice were littermates (n = 20 mice), exposed to either no stimulation (control) or 1 h of continuous light stimulation (sham) with the same overall lux value (~480 lx) as during 40-Hz light stimulation (n = 22 mice). Although the group mean values of the 40-Hz animals tended to be smaller, we did not find a significant difference of Aβ deposition between the 40-Hz-treated and control groups in the neocortex, including the visual cortex (V1), and hippocampus (Fig.

1a–f and Extended Data Fig. 1). In several of these cohorts we also stained for microglia and quantified the overlap between Aβ plaques and microglia[18], and found no significant change in the Pearson correlation between 40-Hz-stimulated ($n = 15$) and control ($n = 15$) mice (Fig. 1g,h). However, when the individual cohorts were examined separately, the 40-Hz group in one cohort (cohort two in Extended Data Fig. 1f) showed a significant reduction in Aβ deposition. A potential explanation for this discrepancy is the large variability of Aβ loads both between the hemispheres and even within the same structures at different anterior–posterior levels (Extended Data Fig. 1a–c and Supplementary Video 1). This large variability of histologically observed Aβ plaques[19] was apparent across the different cohorts, ages, transgenic animals and sexes (Extended Data Fig. 1).

Given the variability and inconsistency of the results on AD pathology after acute 40-Hz stimulation, we also tested the effect of chronic exposure (1 h each day for 7 d)[19] in 7-month-old 5xFAD mice ($n = 7$ male and $n = 5$ female 40-Hz-treated; $n = 7$ male and $n = 4$ female nontreated controls). Mice were euthanized after the seventh day's treatment. One hemisphere of the brain was used for Aβ and microglia immunocytochemistry (Fig. 2a,b) and the other hemisphere for evaluating overall Aβ peptide levels (Aβ40 and Aβ42) (ref. [20]) by Aβ enzyme-linked immunosorbent assay (ELISA) in the hippocampus and V1 (Fig. 2c), as an independent validation for immunocytochemistry. No significant differences were observed by the immunocytochemistry analysis or ELISA between 40-Hz stimulation-treated and control mice (Fig. 2a–c and Extended Data Fig. 2a–d), while Aβ42, but not Aβ40, reduction in V1 reached significance ($P = 0.02$) in the 40-Hz group (Extended Data Fig. 2e)

In vivo changes of Aβ and microglia by two-photon microscopy

To examine the acute effects of 40-Hz light stimulation on Aβ load within the same mice and to reduce the variability inherent in group comparisons, we visualized Aβ load in V1 after intraperitoneal (i.p.) injection of methoxy-X04 (ref. [19]) and imaged Aβ load and microglia with two-photon microscopy (five 7-month-old APP/PS1 mice and four 5xFAD mice) (Supplementary Table 2). Seven of the nine animals were exposed to continuous light for 1 h (sham control) followed by 1 h of rest. After rest, they were stimulated again for 1 h with 40-Hz flicker light pattern (Fig. 3a). During these experiments four images were taken: pre and post sham, and pre and post 40-Hz stimulation. In the remaining two mice, only 40-Hz stimulation was applied (versus no light control). We found no significant difference in the area (percentage) occupied by Aβ load after either sham or 40-Hz stimulation (Fig. 3b,c and Supplementary Video 2), nor in the average area of the individually imaged Aβ load (Fig. 3d,e). After the last image was taken, seven of the imaged mice were euthanized and perfused, and the brain slices were stained with anti-Aβ antibody D54D2 for Aβ load. Histological comparison of these previously imaged brains with those of littermate controls ($n = 3$) showed no significant difference in Aβ plaque load (Fig. 3f).

We crossed 5xFAD mice with macrophage/microglia-specific GFP-expressing Cx3cr1$^{GFP/+}$ mice (Cx3cr1$^{GFP/+}$:5xFAD$^{+/-}$ mice) and examined changes in both Aβ plaques and microglia. The percentage area occupied by microglia in the imaged V1 area did not change either (Fig. 3g,h). In addition, we compared a variety of derived parameters of microglia

before and after 40-Hz stimulation, including area, perimeter, density, number of branches and soma size, and found no effect of 40-Hz stimulation on any of these parameters (Fig. 3i–m).

A 40-Hz stimulation does not entrain native gamma oscillations

The most prominent spontaneous rhythm in the visual system of the mouse is a 4-Hz oscillation[21]. This 4-Hz rhythm can be triggered by visual stimuli[22] and the intrinsic oscillation recruits neurons in several cortical and subcortical structures[23]. To quantify the entrainment of hippocampal neurons by 4-Hz visual stimulation, we analyzed a publicly available dataset[24]. The 4-Hz stimulation not only recruited a large fraction (46%) of V1 neurons, but it also significantly entrained many hippocampal neurons (dentate gyrus: 32%; CA1: 21%; CA3: 18%) and a similar fraction of neurons in the thalamus and brainstem (Extended Data Fig. 3a–d).

Next, we addressed whether 40-Hz stimulation recruits native gamma activity and elicits elevated spiking in V1, entorhinal cortex (EC) and the hippocampus (CA1). In contrast to 4-Hz entrainment, multisite silicon probe recordings revealed that 40-Hz stimulation over the duration of the experiment (15 min control, 30 min stimulation, 15 min control) failed to modify native local field potential (LFP) gamma-band power in V1, EC or CA1 (Fig. 4a–d). Instead, it induced a steady-state response in a narrow band at 40 Hz in V1 (14 sessions in 5 mice) but not in EC (7 sessions in 3 mice) or CA1 (59 sessions in 15 mice; Fig. 4c–e). We took special precautions to eliminate potential artifactual sources of the LFP changes, including shielding the head stages, using a coaxial cable and testing the system for potential crosstalk between the recording and stimulation instruments (Extended Data Fig. 4a–c). For an in-depth analysis, we examined responses of ensembles of single units.

In the majority of the physiological experiments, stimuli were delivered in clusters of 10-s trains (Fig. 4e–h)[17] to be able to examine responses to both train onsets and individual 40-Hz light pulses (‘steady-state’). As expected, light onset robustly engaged neurons in V1, a larger fraction excited and a smaller fraction suppressed (Fig. 4e,f). In the light-onset-responsive subset, the initial transient spiking habituated in <1 s in most neurons (Fig. 4f). In contrast, most neurons in EC and CA1 were not affected (Fig. 4g). To quantify these observations, we used *z*-scores of the cross-correlograms between light train onsets and spike times. Significantly modulated cells had a *z*-score greater than 1.96. While 92 of the 458 V1 neurons (20.1%) responded significantly to light onset, only a small fraction of EC (1.9%; $n = 211$ units) and CA1 hippocampal (0.2%; $n = 463$ units) neurons did so (Fig. 4g,h). As a population, V1 neurons showed an overall significant increase in firing rates during the 10-s-on 40-Hz epochs, compared with the interleaving stimulus-off epochs ($P = 0.0066$; paired *t*-test), whereas changes in EC and CA1 populations were not significant (Extended Data Fig. 5a–c).

Finally, we examined 40-Hz entrainment of individual neurons to individual cycles by constructing peri-event histograms (Fig. 4j) of spikes and testing for modulation using Rayleigh’s test and bootstrapping (Extended Data Fig. 3d). As expected from previous experiments[25], a substantial fraction (132 of 458; 28.8%) of V1 neurons were significantly phase-locked to 40-Hz stimulation (Fig. 4i–l). In contrast, only a small fraction of EC (7

of 211; 3.3%) and hippocampal CA1 (126 of 1,874; 6.7%) neurons showed significant phase-locking of their spikes (Fig. 4k,l). The depth of modulation of significantly entrained neurons was similar across structures (Extended Data Fig. 4e,f), with interneurons being preferentially modulated (Extended Data Fig. 4g).

Behavioral effects of 40-Hz light stimulation

Although humans are perceptually oblivious to 50- or 60-Hz changes of line frequencies or frame refresh rates of old television or computer displays, clear LFP responses can be detected in visual areas[26,27]. To examine whether mice can discriminate 40-Hz flickering from continuous light, we tested 14 intact mice in a modified environment. The original arena was divided into two equal parts; one side was illuminated by the standard 40-Hz stimulation, whereas the other side was lit continuously with the same lux value. Mice spent significantly more time in the continuously lit compartment (Fig. 5a,b and Extended Data Fig. 6a), suggesting that they could distinguish it from 40-Hz and that they perceived the flickering light as unpleasant, as is the case for humans[28].

Because of the possibly aversive aspect of 40-Hz stimulation, we used a photometric method to monitor cholinergic receptor activity in the hippocampus (2,292 trials in 20 sessions, 7 mice)[29]. The 40-Hz stimulation induced elevated activity, independent of motor behavior (Fig. 5c), whereas the onset of continuous light evoked only a transient (<2 s) elevation (Extended Data Fig. 6b).

Discussion

In our physiological experiments, we found that, in contrast to V1, only a small fraction of entorhinal cortical and hippocampal neurons responded to light stimulation or became phase-locked to the 40-Hz pattern, compared with 4-Hz stimulation. Critically, 40-Hz stimulation induced a narrow-band response, distinct from the native gamma oscillation-related spiking of neurons. These observations do not support entrainment of native gamma rhythm as a potential mechanism for affecting Aβ plaques and microglia.

The foundation of 40-Hz stimulation originated from the observation that gamma power during sharp wave ripples was substantially lower in an AD mouse model. It is now known that gamma and ripple frequency oscillations are antagonistic. Both of them are supported by fast firing parvalbumin interneurons so it can be either one or the other[30]. Regardless, the initial experiments concluded that 40-Hz, but not lower frequency, flickering light stimulation can transiently reduce Aβ load and phosphorylated tau proteins in V1[3]. It was suggested that the visual stimulation brings about similar changes in the hippocampus and prefrontal cortex and these beneficial effects were explained by entrainment of gamma oscillations[3–5,10]. The assumed mechanism was the restoration of the well-documented disease-altered oscillations in multiple brain networks[1–3,5,10–12]. Specifically, 40-Hz visual stimulation increased gamma power in V1, hippocampus and prefrontal cortex, along with increased gamma coherence across these structures[3]. In an extension of this approach, auditory 40-Hz stimulation was shown to induce time-locked firing of neurons in the auditory cortex and hippocampus, and to a smaller extent in the prefrontal cortex[5].

Additionally, acute 40-Hz combined visual and auditory stimulation in human patients showed an increase in intracranial electroencephalogram power spectral density[10].

In our experiments, 40-Hz flickering light induced a narrow-band (~1 Hz) LFP response in V1 (see also Figs. 1 and 2 in ref. [4]) but not in the hippocampus and EC. In contrast to V1, only a very small fraction of neurons responded to light onset or were phase-entrained to 40-Hz cycles in the hippocampus and EC. Our findings with 40-Hz stimulation can be contrasted with the effect of 4-Hz, high-contrast stimuli, which resulted in a significant increase of population firing rates and phase-locking of >15% of neurons in V1, dentate gyrus, CA1 and CA3 regions, thalamus and midbrain. This effectiveness is likely due to engaging a native slow oscillation by the stimulation. Previous work has shown that spontaneous 4-Hz oscillation is the most prominent spontaneous rhythm in V1[21], with widespread engagement of thalamic, midbrain and hippocampal activity[23], and can be induced by visual stimulation[22].

Our findings are also in line with previous demonstrations that neurons in limbic structures rapidly habituate to stationary sensory stimuli unless those stimuli acquire behavioral relevance to the organism[14–16]. These LFP findings in rodents extend to the human brain as well. Flickering light stimulation only appeared as a separate narrow-band response (1 Hz) in the power spectrum, even when the flicker frequency was close to the subject's native gamma frequency and without affecting natural gamma-band power[31]. Overall, the available LFP and unit firing observations indicate that sustained steady-state visual responses to external stimuli[25–28] and endogenous gamma oscillations[32] can coexist, but their mechanisms are different[33].

High temporal frequency visual stimuli, although not consciously perceived when their frequency exceeds the subject's critical fusion frequency, can still evoke phase-locked responses in the retina, lateral geniculate nucleus and visual cortical areas in cats, macaques and humans[25,34–38]. The flickering might induce discomfort, eyestrain and headaches[39]. Akin to these observations in humans, we found that mice actively avoided the maze compartment with 40-Hz flicker stimulation, and the potentially aversive nature of the stimulation may explain the sustained increase of acetylcholine release in the hippocampus. In addition to steady-state narrow-band responses, transient sensory stimulation, under some conditions, can also affect the power of natural gamma oscillations[3–5,10]. In visual areas, the most effective stimuli are moving gratings and coherently moving random dot patterns, and the power increase of the native gamma and associated spiking activity vary with visual motion strength[40,41].

Hippocampal neurons can be recruited by several means. In our experiments, 4-Hz stimulation more effectively increased firing rates and phase-locking than 40-Hz stimulation. Cognitive tasks and exploration of the environment are also effective methods for enhancing natural gamma power and coherence across networks in the hippocampus and associated structures[33]. The increased gamma power by these various means is typically larger[42] than those induced by 40-Hz stimulation[31]. It may well be that cognitive training throughout life combats the onset and severity of AD[43], but it remains to be shown whether 40-Hz narrow-band stimulation is more effective or additive.

A secondary goal of our study was to investigate the acute and chronic 40-Hz stimulation-induced changes in brain pathology of AD mice, as reported in the original paper[3]. While in one cohort of mice we found a comparable magnitude of decreased Aβ as in ref. [3], identically treated other cohorts of comparable age (5 months old) and older (7 and 12 months old) mice failed to show consistent differences in Aβ and microglia. This was true after both acute and chronic exposure, regardless of whether we treated APP/PS1 or 5xFAD transgenic, young or old, male or female mice, although in some comparisons the mean values were lower in the 40-Hz-treated animals. One possible source of this discrepancy is the high individual variability of plaque load at the transition age in these strains[19].

We also note some discrepancy between the physiological and histological aspects in previous studies. While 40-Hz exerted a larger effect on neuronal firing and network activity in V1 than in the hippocampus, similar to our observations, Aβ plaque load reduction, prevention of neuronal loss, microglial response and changes in amyloid vasculature were comparable or more effective in the hippocampus, compared with V1[4,5]. Similarly, we did not find a prefe rential effect of 40-Hz stimulation in V1 even in the cohort that showed plaque reduction. In contrast, 4-Hz visual stimulation strongly engaged many brain areas, including the dentate gyrus (our findings), yet low-frequency light or sound stimulation was not able to alter Aβ plaques or other AD markers in previous studies[3–5,10].

Patients with Alzheimer's have decreased power in the delta band (0.5–4 Hz) during sleep and the power of slow waves inversely correlates with memory performance[44]. Decreased delta oscillations were associated with increased Aβ accumulation and tau deposition in the medial prefrontal cortex[45,46], providing support for a link between disruption of slow-frequency activity and AD pathology. In support of these observations in patients with AD, optogenetic stimulation of the neocortex at 4 Hz, but not at a higher frequency, in APP mice for 4 weeks halted Aβ plaque deposition and restored $GABA_A$ and $GABA_B$ receptor levels[47,48]. In another study, optogenetic entrainment of hippocampal neurons bilaterally at theta frequency (10 Hz) improved memory in a novel object recognition task in APP mice[49]. In contrast, direct optogenetic stimulation of the hippocampus of rTg4510 mice at gamma frequency (30 Hz), for three times 1 min per day, five times per week for 4 weeks (60 stimulations total), enhanced human tau in the pyramidal cell bodies, suggesting that elevated spiking activity exacerbates AD pathology[50]. In V1 of normal mice, flickering light stimulation at 60 Hz, but not at 40 Hz or 8 Hz, reduced perineuronal nets around parvalbumin-containing interneurons[51]. Finally, a recent pilot study in six patients with early AD used Pittsburgh compound B positron-emission tomography for tracing ([^{11}C] *N*-methyl [^{11}C] 2-(4′methylaminophenyl)-6-hydroxy-benzothiazole (PiB)) to quantify Aβ deposition. It found no postintervention effects in the V1 or in four other cortical regions following 10 d of 2 h of daily 40-Hz flickering light therapy[52]. In sum, delta-frequency stimulation can be as effective in altering Aβ accumulation and tau deposition as 40 Hz. Furthermore, it appears that gamma frequency stimulation can both decrease and increase AD pathology, depending on the exact conditions.

To examine the acute effects of 40-Hz stimulation more directly, we monitored Aβ plaques and microglia before and immediately after light stimulation, using two-photon imaging in the same animal. In this within-subject design, we did not find reliable changes in Aβ

plaque deposition or microglia in response to flickering light stimulation. Moreover, when the brains of the same mice were examined histologically, they did not differ significantly from no-treatment controls.

In summary, exploitation of the possible beneficial effects of 40-Hz sensory stimulation will require further scrutiny. Our failure to observe changes consistently and reliably in AD pathology after acute or chronic exposure should not be taken as evidence against potential beneficial outcome in mice or humans[10] chronically exposed to combined 40-Hz flickering light and sound stimulation[4,5]. We note that some histopathological and ELISA measures showed some improvement after 40-Hz stimulation, and decrease of Aβ42 in V1 reached statistical significance. It remains a possibility that some unidentified experimental details are responsible for our failure to replicate the beneficial effect of flickering light stimulation on Aβ plaques and microglia. Yet, our findings suggest that entrainment of natural gamma-band oscillations is not a likely mechanism for reducing AD pathology. A search for alternative mechanisms is thus warranted.

Online content

Any methods, additional references, Nature Portfolio reporting summaries, source data, extended data, supplementary information, acknowledgements, peer review information; details of author contributions and competing interests; and statements of data and code availability are available at https://doi.org/10.1038/s41593-023-01270-2.

Methods

Immunohistochemistry (IHC) experiments

All experiments were approved by the Institutional Animal Care and Use Committee at New York University Langone Medical Center. Mice were housed in optimal ambient temperature (70 °F) and humidity (50%) conditions. We used 5-, 7- and 12-month-old APP/PS1 hemizygotic mice (Jax Stock, no. 004462) and 4- and 7-month-old 5xFAD mice (034840-JAX) in these experiments, based on previous findings in ref. [3]. Mice were kept in their home-cage and allowed to acclimate to the experimental room for several minutes, followed by continuous 40-Hz visual stimulation for 1 h. After stimulation, the animals were deeply anesthetized with isoflurane and perfused transcardially, first with 0.9% PBS solution, followed by 4% paraformaldehyde solution. Brains were postfixed overnight in 4% paraformaldehyde solution at 4 °C and washed in PBS before sectioning. Brains were sectioned into 10-μm-thick slices (Leica Vibratome). Sections were stained with anti-Aβ antibody D54D2 (1:10,000; Cell Signaling Technologies, cat. no. 8243), anti-Iba1 (1:1,000; Wako Chemicals, cat. no. 019–19741) and DAPI, following the description in ref. [17]. Secondary antibodies Opal 520 fluorophore (1:150; Akoya, no. FP1487001KT) and Opal 690 fluorophore (1:150; Akoya, no. FP1497001KT) were used. Images were acquired using an epifluorescence microscope at ×40 (Bx61VS, Olympus). Quantification of Aβ was done in Fiji ImageJ2 by an experimenter blind to conditions and experimental design. Four coronal sections per animal, covering V1, lateral cortex and hippocampus (Fig. 1b,c and Extended Data Fig. 1d), were used for quantifications. To quantify the fraction of microglia overlapping with Aβ, we used the polygon selection in ImageJ2 to crop the V1 region (1,476

height × 1,509 width) and the JACop plug-in to acquire the Pearson correlation coefficient (PCC).

ELISA method

The hemisphere that was not used for histological evaluation was sliced into 50-μm-thick sections. The V1 and hippocampus were micro-dissected from eight sections per animal. Extraction of protein from fixed tissue was done by adding 500 mM Tris-HCl and 2% SDS to the fixed-tissue lysis buffer and heating the 50-μm-thick fixed-tissue sections for 120 min (ref. [20]). Using an Invitrogen ELISA kit, Aβ42 and Aβ40 (human) were quantified blindly and normalized to total protein in samples via Bradford protein assay. Aβ42 was repeated twice to confirm the reliability of the ELISA methodology (Extended Data Fig. 2e).

In vivo transcranial two-photon imaging

Surgical preparation for in vivo two-photon imaging in awake, restrained mice: $Cx3cr1^{GFP/+}$ mice (Jax Stock: 005582) were used to generate the $Cx3cr1^{GFP/+}$:$5xFAD^{+/-}$mice. In preparation for imaging, APP/PS1 and $Cx3cr1^{GFP/+}$:$5xFAD^{+/-}$ mice were anesthetized with an i.p. injection of a mixture of ketamine (100 mg kg^{-1}) and xylazine (15 mg kg^{-1}) to implant a head holder. The mouse head was shaved, and the skull was exposed with a midline scalp incision. The periosteum tissue over the skull surface was removed without damaging the temporal and occipital muscles. A head holder, composed of one metal bar, was attached to the animal's skull to help restrain the mouse's head and reduce motion-induced artifacts during imaging. A region (~0.5 mm in diameter) was located over the V1 based on stereotaxic coordinates (2.27 mm posterior to the bregma and 2 mm lateral from the midline) and marked with a pencil. A thin layer of cyanoacrylate-based glue was first applied to the top of the skull surface, and the head holder was mounted on top of the skull with dental acrylic cement such that the marked skull region was exposed. After surgery, the mice were returned to their home-cage and monitored daily during a recovery period of 5 d before two-photon imaging. At 18–24 h before starting the experiment, the mice received an i.p. injection of methoxy-X04 (6.66 mg kg^{-1})[54]. At 3 h before two-photon imaging acquisition, the mice were transiently anesthetized with an i.p. injection of ketamine to create a thinned-skull window over the V1. The detailed procedures for preparing a thinned-skull window for two-photon imaging have been described in detail previously[55]. In brief, a high-speed micro-drill was used over the previously marked region to remove the acrylic glue layer as well as the external layer of the compact bone and most spongy bone. The skull was immersed in artificial cerebrospinal fluid to avoid heating the cortex during drilling. A microsurgical blade was then used to continue the thinning process until the cranial surface was approximately 20–50 μm in thickness. Once the mice were fully recovered from the anesthesia, we started two-photon imaging data acquisition.

Two-photon imaging data acquisition and analysis: In vivo imaging was performed with an Olympus Fluoview 1000 two-photon system, equipped with a Ti:Saphire laser (MaiTai DeepSee, Spectra Physics) and tuned to 755 and 920 nm for visualizing methoxy-X04-labeled plaques and $Cx3cr1^{GFP/+}$ microglia, respectively. For each frame, a 512 × 512-pixel, digital zoom ×1 image was taken from a 508 × 508 μm^2 region of interest. A *z*-stack (2 μm in step size) over the V1 was taken before and after visual stimulation (continuous

light and 40-Hz). The average laser power on the tissue sample was progressively increased from ~10–15 mW to 50–60 mW as the focal plane went deeper into the tissue, until reaching a depth of 100 μm below the pia. All experiments were performed using a ×25 objective (numerical aperture 1.1) immersed in an artificial cerebrospinal fluid solution or gel. All images were acquired at frame rates of 1 Hz (1-μs pixel dwell time). Seven of nine animals were exposed to continuous light for 1 h (sham) then allowed to rest for 1 h, and then stimulated for 1 h with 40-Hz flicker light pattern (Supplementary Video 2). During these experiments, four images were taken: pre and post sham, and pre and post 40-Hz stimulation. After the last image, mice were euthanized and perfused, and brain slices were stained with Iba1 and D54D2. Two of the six Cx3cr1$^{GFP/+}$:5xFAD$^{+/-}$ mice were imaged only twice, before and after 40-Hz stimulation. Image acquisition was performed using FV10-ASW v.2.0 software and analyzed post hoc using Fiji ImageJ2. Percentage area of plaques and microglia was quantified using the same method described above for the IHC quantification. The Microglia Morphology Analysis plug-in[53] was used to quantify the morphological changes occurring across 40-Hz flicker and sham conditions.

Electrophysiological experiments

Surgery: Mice (adult C57BL/6J and APP/PS1 male and female, 20–30 g, 3–6 months old) were kept in the vivarium on a 12-h reverse light/dark cycle. Mice were housed two to three animals per cage before surgery and individually after surgery.

Mice were anaesthetized using isoflurane and placed in a stereotactic frame as described previously[33]. Craniotomies were made for the hippocampus CA1 (AP: 1.55 mm, ML: 1 mm, DV: 1.3 mm), V1 (AP: 4.35 mm, ML: 2.5 mm, DV: 0.5 mm) or EC (AP: 4.7 mm, ML: 3.5 mm, DV: 2.5 mm). Silicon probes (Cambridge Neurotech or NeuroNexus) were mounted on custom-made three-dimensionally (3D)-printed drives and were inserted into the target brain region. Drives and a 3D-printed head cap were cemented to the skull with dental cement. Post implantation, craniotomies were covered with sterile wax. The copper mesh surrounding the 3D-printed head cap was connected to a screw in the skull and served as a Faraday cage to prevent photodynamic contamination from the 40-Hz visual stimulation. Post surgery, the probe was moved in the brain until the target region was physiologically identified.

Neuropixels data.

The 4-Hz gratings stimulation data presented here used data from the Allen Brain Institute Visual Coding dataset publicly available at https://allensdk.readthedocs.io/en/latest/visual_coding-neuropixels.html (AI Dataset). The stimuli were two 150-ms checkerboard patterns separated by 500-ms no-stimulation intervals.

The 40-Hz visual stimulation: In the physiological experiments, mice were used in multiple sessions, separated by a minimum of 1 d. They were allowed to acclimate to the recording room for 15–30 min before stimulation. Recording time was between 14:00 and 17:00 during the animal's wake cycle. Mice were awake but mainly immobile during the light stimulation protocol. Arduino-powered light-emitting diodes (LEDs) were programmed to flicker at 12.5 ms on and 12.5 ms off. In several physiological experiments, interleaving 10

s on and 10 s off, 40-Hz light trains were used to examine both light-onset responses of neurons and their phase-entrainment to the 40-Hz stimuli (steady-state responses). A 10-min baseline was recorded first, followed by 40-Hz stimulation for 30 min and concluding with a second 10 min of no-stimulation control epoch.

Electrophysiology data acquisition.

Electrophysiological recordings were conducted using an Intan RHD2000 interface board and 64-channel digital head stages with sampling at 20 kHz (IntanTech), and visualized using the Neurosuite software. The Intan board was grounded, and a copper mesh placed under the recording cage was connected to the ground of the Intan board. The Arduino stimulation control system was also grounded to the Intan.

Spike sorting and unit modulation.

Neuronal spikes were segregated using KiloSort2 (https://github.com/cortexlab/KiloSort) (ref. [56]) and manual curating sessions using Phy (https://github.com/kwikteam/Phy). Putative excitatory and inhibitory neurons were separated based on their autocorrelograms and waveform characteristics using CellExplorer[57].

To determine spike-locking to the phase of 40-Hz stimulation, we used two different methods. First, Rayleigh's test for circular data to determine whether neuronal spikes had a significant phase preference to the 40-Hz stimulation ($Z = R^2/n$), where n equals the number of spikes and R is the mean resultant vector length[58]. Second, we did bootstrap hypothesis testing. Here, 1,000 randomly shuffled 40-Hz pulses were generated, and a distribution of the vector length response was generated. Significantly modulated cells had vector lengths greater than 5% of the distribution. Neurons that had a modulation P value < 0.05 in both Rayleigh's test and bootstrap are displayed in the figures.

Spectral analysis of LFP.

Wavelet and spectral analysis of the LFP were analyzed throughout the experiment. The LFP was downsampled at 1,250 Hz and low-pass-filtered at 450 Hz. The power spectral density was computed using Welch's average. The time–frequency spectrogram was computed between 2 and 100 Hz using a moving window of 2 s (ref. [33]).

Behavioral task

The animal's home-cage was modified to have two compartments by using black cardboard with a small opening for the animal to move between compartments. One compartment was exposed to 40-Hz visual stimulation and the other was exposed to continuous white light. The LEDs were calibrated to have the same lux value (~480 lx) light exposure in the two compartments. Mice were allowed to acclimate to the room for 30 min before the onset of the experiment. The lights were turned on and mice were allowed to explore for 10 min. The time spent in each compartment was calculated.

Fiber photometry for acetylcholine experiments

Virus injection and fiber implantation: The skull was exposed under antiseptic conditions using local anesthesia with bupivacaine/lidocaine, and holes were drilled above the

hippocampal CA1 region: AP: −2.3 mm, ML: ±2.00 mm. A glass pipette (30–50-μm tip) connected to a Nanoject II/Nanoliter 2000 microinjector (Drummond Scientific or WPI) was used to inject 0.1 μl of virus solution (AAV-hSyn-Ach3.0; Vigene Biosciences) at 1.2-mm and 1.5-mm depths in CA1, over 15 min. Afterwards, the injection pipette was removed slowly (0.1-mm then 0.5-mm steps, 10-min waiting periods between each) and the scalp was sutured. After 21 d, a 400-μm-diameter optical fiber was implanted at 1.5-mm depth and 200–300 μm above the injection site to collect the emission fluorescence signal ($n = 7$ mice).

Ach3.0 fluorescence signal and fiber photometry: During recording, a 400-Hz square wave with 60% duty cycle was used to drive the LED (470 nm) by a signal generator (Rigol DG4062 Arbitrary Waveform Generator) and excite the Ach3.0 GRAB sensor[29]. The LED driver (LEDD1B) and fiber-coupled LED (M470F3) were obtained from Thorlabs. The applied power measured from the mono fiberoptic patchcord (FC-MF1.25) tip was 30 ~ 60 μW, and from the optical fiber (FP400URT or FP200URT) 80–95% of the power entered the brain (measured by PM100D from Thorlabs, in air). The emission light of Ach3.0 fluorescence in the dorsal hippocampus traveled back through the same optical fiber, was bandpass filtered (500–550 nm, Minicube, FMC3-e(460–490) F(500–550)_S, Doric), passed through a low-pass filter (Model 440 Instrumentation Amplifier) at 20 Hz, was detected by a Femtowatt Silicon Photoreceiver (Newport, 2151) and was recorded using a real-time processor (CED, 1401). The Ach3.0 fluorescence response was obtained using the equation $\Delta F/F = (F - F\_0)/F\_0$, in which F_0 is the baseline signal detected by a fifth-order polynomial fitting[59].

Mice were allowed to acclimate to the room for 15 min. A 20-min Ach baseline was recorded first, followed by 40-Hz stimulation (10 s on, 10 s off; $n = 6$ mice) or continuous white LED (10 s on, 10 s off; $n = 5$ mice) for 40 min and concluding with another 20 min of no-stimulation control epoch.

Statistics and reproducibility

Mice were randomly grouped considering equal distribution of sex. Additionally, we used various tests and genetic lines to replicate our negative findings. Data collection was not preformed blinded to the subject conditions. However, data analysis was performed blinded. All statistical analyses were performed with standard MATLAB functions and statistical tests. No data were excluded from the analysis and details pertaining to the exact numbers of replications, animals and units are given in the text and figures. Unless otherwise noted, group comparison was performed using a nonparametric two-tailed Wilcoxon's rank-sum test. Parametric tests were used when the data passed normality and equal variance tests (Kolmogorov–Smirnov test and Bartlett test, respectively). P values for Pearson correlations were computed using a Student's t distribution for a transformation of the correlation. No statistical methods were used to predetermine sample sizes but our sample sizes are greater than those reported in previous publications[3–7,17].

Reporting summary

Further information on research design is available in the Nature Portfolio Reporting Summary linked to this article.

Extended Data

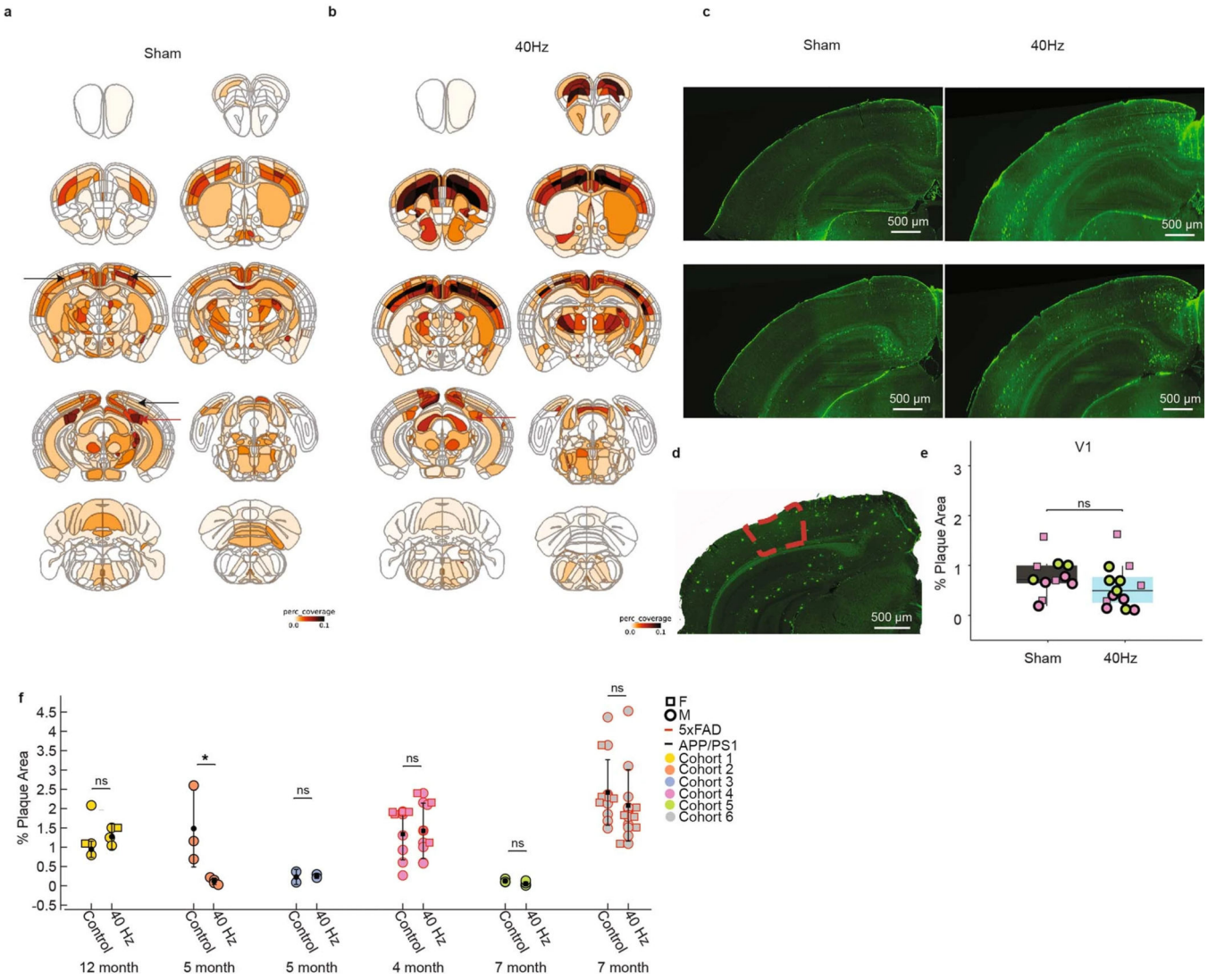

Extended Data Fig. 1 |. Histological analysis.

a, **b**) Heatmaps of Aβ plaque load in various coronal sections in 5xFAD mice after sham (a) and 40-Hz flicker (b) stimulation. **c**) Representative coronal sections of Aβ expression (LifeCanvas Technologies, Cambridge, MA 02141). Was replicated in n = 2 mice. **d**) Posterior visual cortex section (marked by red dash lines), used for quantification of V1. **e**) Group difference (medians, interquartile ranges, maxima and minima) of the percent area occupied by plaques after sham (n = 11 mice) and 40-Hz flicker (n = 13 mice) stimulation (ns, not significant by Wilcoxon test: p = 0.12). **f**) Cortex plaque load variability among six cohorts (mean + /− s.d; two-sided Wilcoxon test; p = 0.915, p = 0.0368, p = 0.879, p = 0.988, p = 0.0878, p = 0.379; ns, not significant).

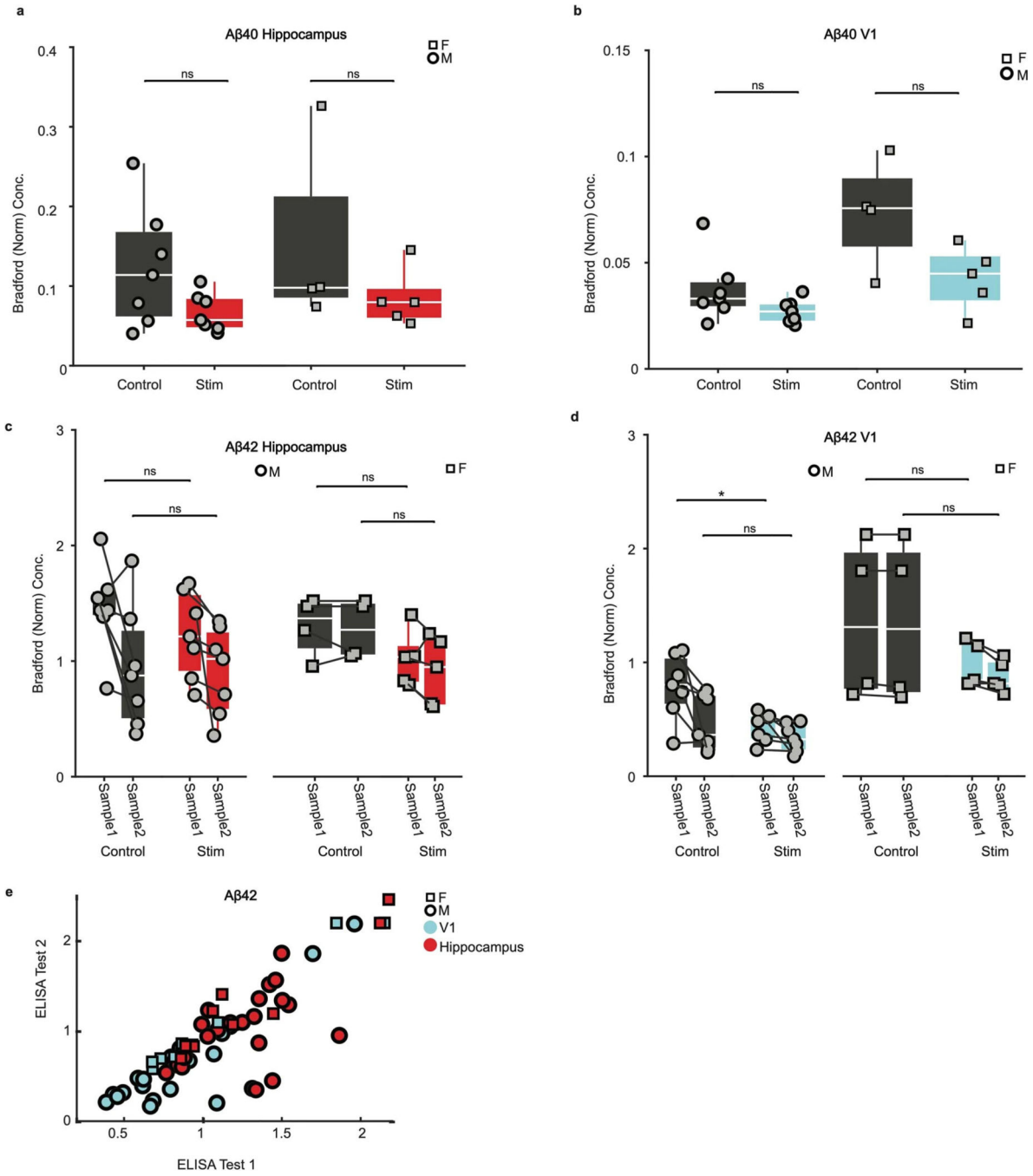

Extended Data Fig. 2 |. ELISA analysis by groups.

a, **b**) Group difference (medians, interquartile ranges, maxima and minima) Aβ40 peptide levels in the (a) hippocampus and (b) V1 separated by sex (ns, not significant; two-sided Wilcoxon test). (n = 7 male and n = 5 female 40-Hz treated; n = 7 male and n = 4 female non-treated controls) **c**, **d**) Group difference (medians, interquartile ranges, maxima and minima) Aβ42 peptide levels in the (c) hippocampus (p = 0.38; p = 1;p = 0.19; p = 0.19 two-sided Wilcoxon Test) and (d) V1 (p = 0.02; p = 0.46;p = 0.68; p = 0.73; two-sided Wilcoxon Test) separated by sex and ELISA test. To test the reliability and consistency of

the ELISA method, we performed two separated analyses for Aβ42 from the same aliquot samples on different days separated by one week (sample 1, sample2). The corresponding aliquots in the two tests are connected by lines. (n = 7 male and n = 5 female 40-Hz treated; n = 7 male and n = 4 female non-treated controls) **e**) The correlation between the two ELISA tests in c and d. Two conclusions may be drawn from this repeated analysis. First, the two tests were correlated strongly and significantly (R = 0.78). Second, the values of the second ELISA test were, on average, lower. This latter observation suggests that some epitope degradation of the sample may take place with time. These findings points to further potential sources of variability across studies, which may have different delays between tissue processing and ELISA Analysis.

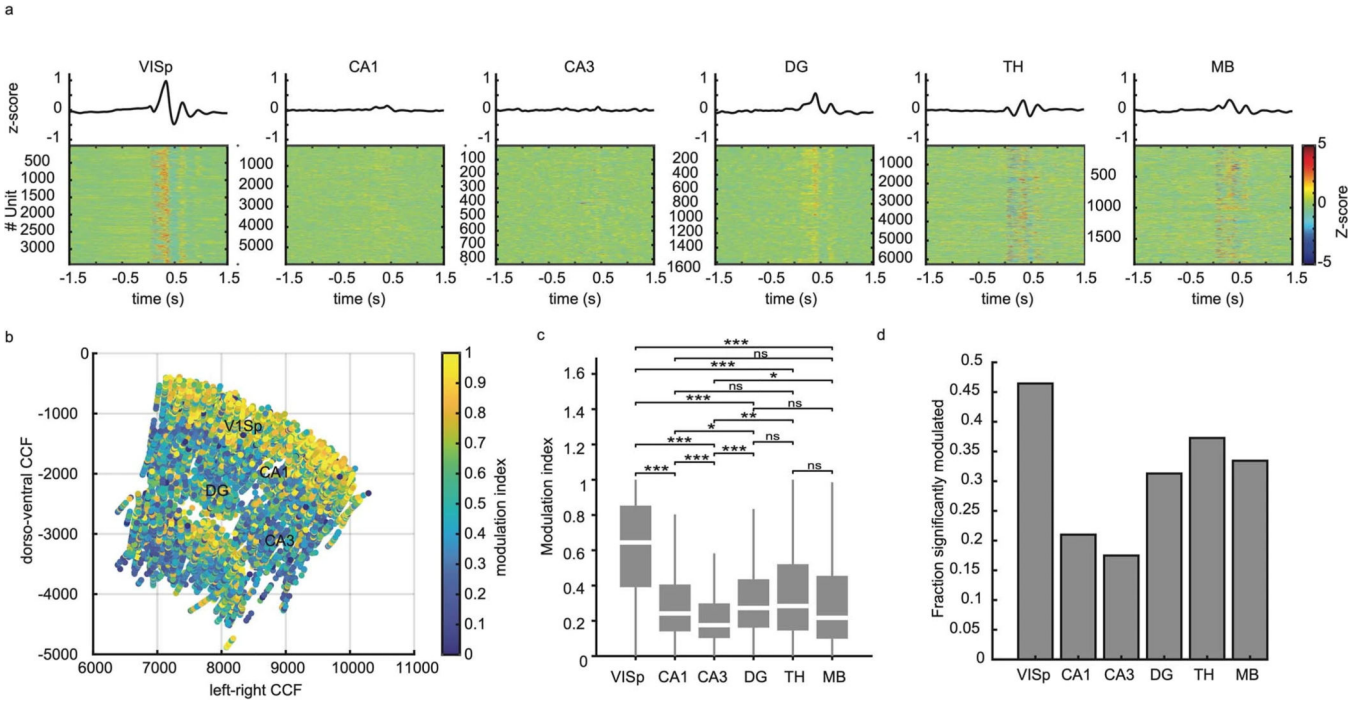

Extended Data Fig. 3 |. Allen Brain Institute 4-Hz light response.

a) Peristimulus time histograms showing the responses of individual neurons (bottom panels) and the average (mean ± s.e.m.) response per area, from primary visual cortex (VISp), the 3 major hippocampal areas (DG, dentate gyrus), the thalamus (TH) and midbrain (MB). **b**) Anatomical locations of 35,910 units included in the dataset, color coded according to their modulation index. **c**) Box and whisker plot (medians, interquartile ranges, maxima and minima) showing the distributions of modulation index in the different areas p = 0, p = 0, p = 0, p = 0, p = 0, p = 4.9e-14, p = 0.013,p = 0.999,p = 0.970, p = 8.97e-19, p = 0.0006, p = 0.0434, p = 0.940, p = 0.359, p = 0.962 for VISp-CA1, VISp-CA3, VISp-DG, VISp-TH, VISp-MB, CA1-CA3, CA1-DG, CA1-TH, CA1-MB, CA3-DG, CA3-TH, CA3MB, DG-TH,DG-MB,TH-MB, respectively; KW; *p < 0.05, **p < 0.01, ***p < 0.001. **d**) Bar graph shows the fractions of significantly modulated cells per area (VISp: 1597/3439; CA1: 1225/5833; CA3:145/835; TH:2329/6249; MB: 638/1908) (n = 49 mice).

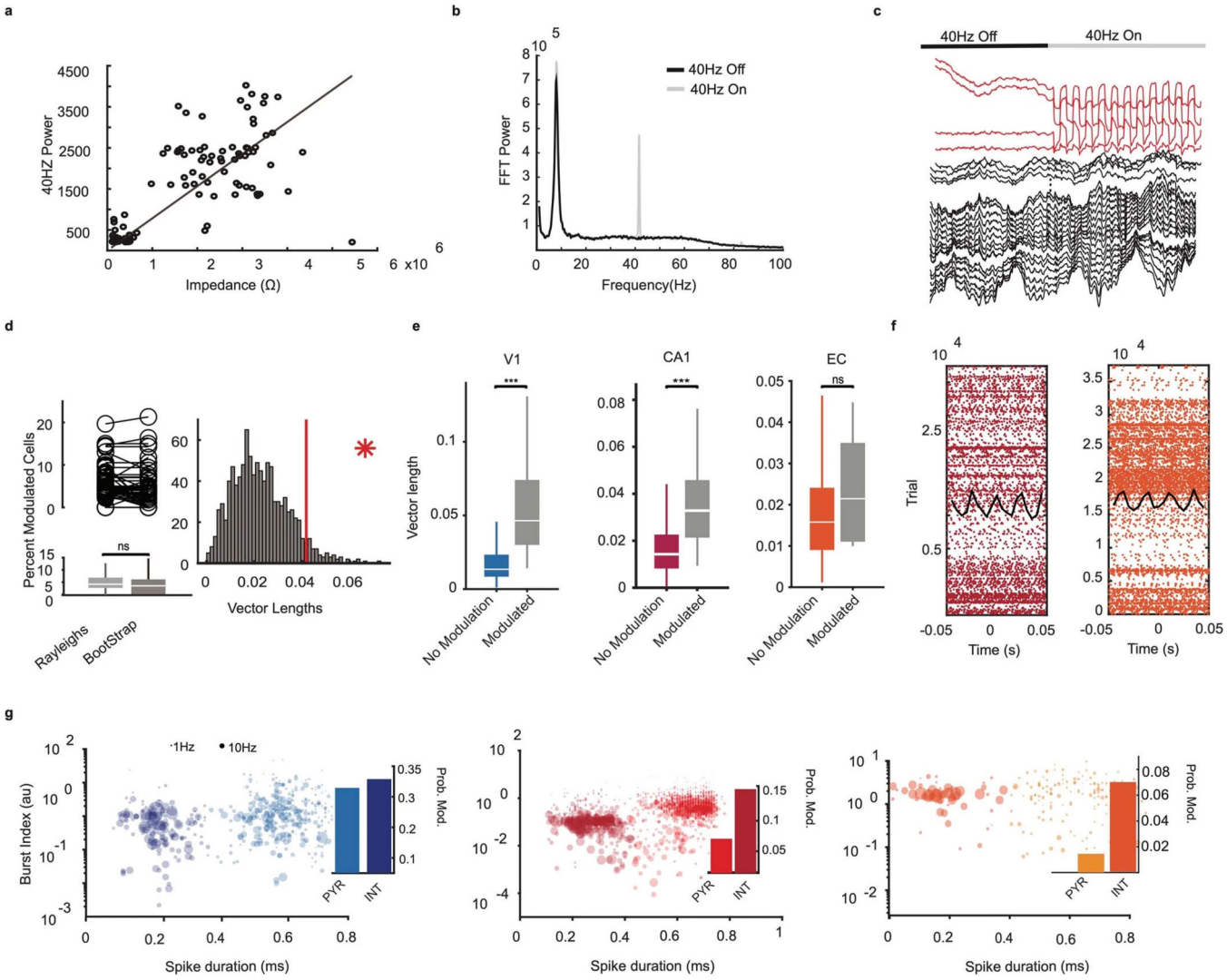

Extended Data Fig. 4 |. Electrophysiological methods.

a) Relationship between electrode impedance and 40-Hz power in the hippocampus. Note that artifactual 40-Hz power can occur at high impedance sites. **b**) Power spectra in a high impedance channel in the hippocampus during 40-Hz stimulation and no-stimulation epochs (10 s on, 10 s off). Note large peak at 40-Hz during stimulation. **c**) Example artifacts at a high-impedance channels (red traces) in the hippocampus show 40-Hz when the light is turned on. **d**) Comparison (medians, interquartile ranges, maxima and minima) of the two methods we used to quantify phase modulation of spikes: bootstrap and Rayleigh's methods (Example from the hippocampus; ns, nonsignificant p = 0.193; two-sided Wilcoxon test). Vector length distribution. Vertical red lines separate nonsignificant and significant events. (59 sessions in 15 mice). **e**) Significant difference (medians, interquartile ranges, maxima and minima) in the vector lengths of neurons statistically modulated by 40-Hz in different brain regions. Note that despite very few CA1 and EC neurons show significant phase-locking to 40-Hz stimuli (Fig. 2), the few that do show comparable vector lengths in all three structures (***p < 0.001; V1:p = 3.12e-41;CA1: p = 1.6e-30; EC: p = 0.239; two-sided Wilcoxon test) (V1 = 14 sessions in 5 mice, EC = 7 sessions in 3 mice, CA1

= 59 sessions in 15 mice). **f**) Example raster plots of significantly modulated putative interneurons in CA1 (red) and EC (orange) regions. **g**) Separation of putative pyramidal cells from interneurons using spike duration and burst index. Bar graphs show the fraction of significantly modulated putative pyramidal cells and interneurons.

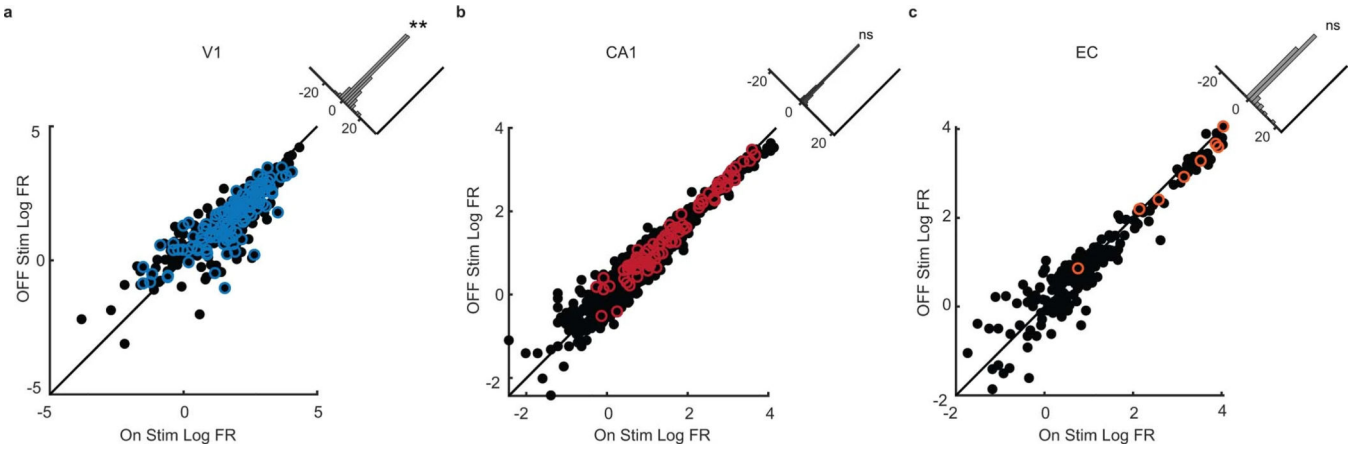

Extended Data Fig. 5 |. Firing rates changes during stead state driving at 40-Hz stimulation.
Firing rates of all neurons during onset and offset of 40-Hz trains every 10 second for the visual cortex (**a**; two-sided paired t-test; p = 0.0066), hippocampus (**b**; two-sided paired t-test; p = 0.2581), and entorhinal cortex (c; two-sided paired t-test; p = 0.2629), respectively. Bin size= 0.005 s. 40-Hz modulated cells are marked by color circles.

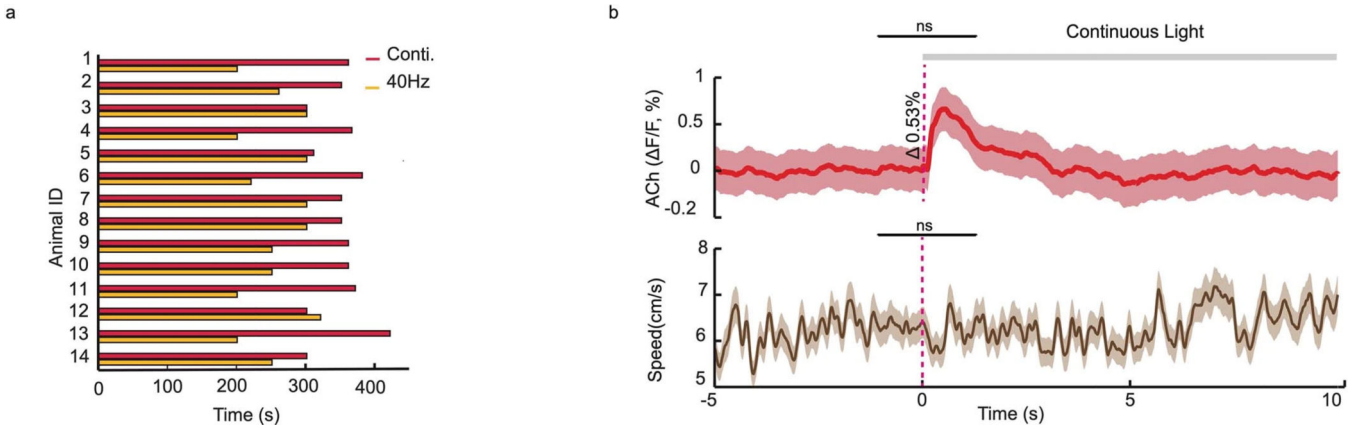

Extended Data Fig. 6 |. Aversive response to 40-Hz flicker and control Ach.
a) Time spent in the 40-Hz compartment versus in the compartment with continuous light (n = 14 mice). **b**) Ach response to continuous white light (mean + /− s.e.m; $p = 0.59$, two-tailed paired t-test; n = 5 mice). Note lack of sustained activity, in contrast to the sustained Ach activation with 40-Hz flickering light (Fig. 4).

Supplementary Material

Refer to Web version on PubMed Central for supplementary material.

Acknowledgements

We thank D. Adler, M. Valero, E. M. Sigurdsson, the Experimental Pathology research core at NYU and Life Canvas for their experimental support. This work was supported by NRSA grant no. 5TL1TR001447–07 (M.S.), a DFG Walter Benjamin fellowship (grant no. NI 2057/1–1) (N.N.), the Alzheimer's Association grant no. AARFD-17–533584 (A.M.-A.), grant no. R01 AG075840 (M.J.S.), the Fisher Center for Alzheimer's Research Foundation (M.J.S.) NIH grants no. MH122391 and no. U19 NS107616 (G.B.).

Data availability

The data that support the main findings of this study are publicly available on the Buzsáki Lab web page (https://buzsakilab.com/wp/resources/). Supplementary data used from the Allen Brain Institute can be found at https://allensdk.readthedocs.io/en/latest/visual_coding_neuropixels.html. Source data are provided with this paper.

Code availability

The code used for this study was adapted from the buzcode repository (https://github.com/buzsakilab/buzcode).

References

1. Llinás RR, Ribary U, Jeanmonod D, Kronberg E & Mitra PP. Thalamocortical dysrhythmia: a neurological and neuropsychiatric syndrome characterized by magnetoencephalography. Proc. Natl Acad. Sci. USA 96, 15222– 15227 (1999). [PubMed: 10611366]
2. Krook-Magnuson E, Gelinas JN, Soltesz I & Buzsáki G. Neuroelectronics and biooptics: closed-loop technologies in neurological disorders. JAMA Neurol. 72, 823–829 (2015). [PubMed: 25961887]
3. Iaccarino HF et al. Author correction: gamma frequency entrainment attenuates amyloid load and modifies microglia. Nature 562, E1 (2018). [PubMed: 30046102]
4. Adaikkan C et al. Gamma entrainment binds higher-order brain regions and offers neuroprotection. Neuron 102, 929–943.e8 (2019). [PubMed: 31076275]
5. Martorell AJ et al. Multi-sensory gamma stimulation ameliorates Alzheimer's-associated pathology and improves cognition. Cell 177, 256–271.e22 (2019). [PubMed: 30879788]
6. Shen Q et al. Gamma frequency light flicker regulates amyloid precursor protein trafficking for reducing β-amyloid load in Alzheimer's disease model. Aging Cell 21, e13573 (2022). [PubMed: 35199454]
7. Park SS et al. Combined effects of aerobic exercise and 40-Hz light flicker exposure on early cognitive impairments in Alzheimer's disease of 3×Tg mice. J. Appl. Physiol. 132, 1054–1068 (2022). [PubMed: 35201933]
8. Yao Y et al. Non-invasive 40-Hz light flicker ameliorates Alzheimer's-associated rhythm disorder via regulating central circadian clock in mice. Front. Physiol. 11, 294 (2020). [PubMed: 32390857]
9. Bero AW et al. Neuronal activity regulates the regional vulnerability to amyloid-β deposition. Nat. Neurosci. 14, 750–756 (2011). [PubMed: 21532579]
10. Chan D et al. Gamma frequency sensory timulation in probable mild Alzheimer's dementia patients: results of a preliminary clinical trial. PLoS ONE 17, e0278412 (2022). [PubMed: 36454969]
11. Park SS et al. Physical exercise during exposure to 40-Hz light flicker improves cognitive functions in the 3xTg mouse model of Alzheimer's disease. Alzheimers Res. Ther. 12, 62 (2020). [PubMed: 32434556]
12. Zheng L et al. Rhythmic light flicker rescues hippocampal low gamma and protects ischemic neurons by enhancing presynaptic plasticity. Nat. Commun. 11, 3012 (2020). [PubMed: 32541656]

13. Etter G et al. Optogenetic gamma stimulation rescues memory impairments in an Alzheimer's disease mouse model. Nat. Commun. 10, 5322 (2019). [PubMed: 31757962]
14. Aronov D, Nevers R & Tank DW. Mapping of a non-spatial dimension by the hippocampal-entorhinal circuit. Nature 543, 719–722 (2017). [PubMed: 28358077]
15. Thompson RF. The neurobiology of learning and memory. Science 233, 941–947 (1986). [PubMed: 3738519]
16. Tiitinen H et al. Selective attention enhances the auditory 40-Hz transient response in humans. Nature 364, 59–60 (1993). [PubMed: 8316297]
17. Singer AC et al. Noninvasive 40-Hz light flicker to recruit microglia and reduce amyloid beta load. Nat. Protoc. 13, 1850– 1868 (2018). [PubMed: 30072722]
18. Bolte S & Cordelières FP. A guided tour into subcellular colocalization analysis in light microscopy. J. Microsc. 224, 213–232 (2006). [PubMed: 17210054]
19. Forner S et al. Systematic phenotyping and characterization of the 5xFAD mouse model of Alzheimer's disease. Sci. Data 8, 270 (2021). [PubMed: 34654824]
20. Thacker JS et al. Unlocking the brain: a new method for western blot protein detection from fixed brain tissue. J. Neurosci. Methods 348, 108995 (2021). [PubMed: 33202258]
21. Senzai Y, Fernandez-Ruiz A & Buzsáki G. Layer-specific physiological features and interlaminar interactions in the primary visual cortex of the mouse. Neuron 101, 500–513.e5 (2019). [PubMed: 30635232]
22. Einstein MC, Polack PO, Tran DT & Golshani P. Visually evoked 3–5 Hz membrane potential oscillations reduce the responsiveness of visual cortex neurons in awake behaving mice. J. Neurosci. 37, 5084–5098 (2017). [PubMed: 28432140]
23. Nitzan N, Swanson R, Schmitz D & Buzsáki G. Brain-wide interactions during hippocampal sharp wave ripples. Proc. Natl Acad. Sci. USA 119, e2200931119 (2022). [PubMed: 35561219]
24. Steinmetz NA, Zatka-Haas P, Carandini M & Harris KD. Distributed coding of choice, action and engagement across the mouse brain. Nature 576, 266–273 (2019). [PubMed: 31776518]
25. Lyskov E, Ponomarev V, Sandström M, Mild KH & Medvedev S. Steady-state visual evoked potentials to computer monitor flicker. Int. J. Psychophysiol. 28, 285–290 (1998). [PubMed: 9545663]
26. Williams PE, Mechler F, Gordon J, Shapley R & Hawken MJ. Entrainment to video displays in primary visual cortex of macaque and humans. J. Neurosci. 24, 8278–8288 (2004); erratum 24, 10034 (2004). [PubMed: 15385611]
27. Krolak-Salmon P et al. Human lateral geniculate nucleus and visual cortex respond to screen flicker. Ann. Neurol. 53, 73–80 (2003). [PubMed: 12509850]
28. Lee K et al. Optimal flickering light stimulation for entraining gamma waves in the human brain. Sci. Rep. 11, 16206 (2021). [PubMed: 34376723]
29. Jing M et al. An optimized acetylcholine sensor for monitoring in vivo cholinergic activity. Nat. Methods 17, 1139–1146 (2020). [PubMed: 32989318]
30. Oliva A, Fernández-Ruiz A, Fermino de Oliveira E & Buzsáki G. Origin of gamma frequency power during hippocampal sharp-wave ripples. Cell Rep. 25, 1693–1700.e4 (2018). [PubMed: 30428340]
31. Duecker K, Gutteling TP, Herrmann CS & Jensen O. No evidence for entrainment: endogenous gamma oscillations and rhythmic flicker responses coexist in visual cortex. J. Neurosci. 41, 6684–6698 (2021). [PubMed: 34230106]
32. Wang XJ & Buzsáki G. Gamma oscillation by synaptic inhibition in a hippocampal interneuronal network model. J. Neurosci. 16, 6402–6413 (1996). [PubMed: 8815919]
33. Fernández-Ruiz A et al. Gamma rhythm communication between entorhinal cortex and dentate gyrus neuronal assemblies. Science 372, eabf3119 (2021). [PubMed: 33795429]
34. Berman SM, Greenhouse DS, Bailey IL, Clear RD & Raasch TW. Human electroretinogram responses to video displays, fluorescent lighting, and other high frequency sources. Optom. Vis. Sci. 68, 645–662 (1991). [PubMed: 1923343]

35. Herrmann CS. Human EEG responses to 1–100 Hz flicker: resonance phenomena in visual cortex and their potential correlation to cognitive phenomena. Exp. Brain Res. 137, 346–353 (2001). [PubMed: 11355381]
36. Fylan F & Harding GF. The effect of television frame rate on EEG abnormalities in photosensitive and pattern-sensitive epilepsy. Epilepsia 38, 1124–1131 (1997); erratum 39, 453 (1998). [PubMed: 9579959]
37. Gur M & Snodderly DM. A dissociation between brain activity and perception: chromatically opponent cortical neurons signal chromatic flicker that is not perceived. Vis. Res. 37, 377–382 (1997). [PubMed: 9156168]
38. Ghose GM & Freeman RD. Oscillatory discharge in the visual system: does it have a functional role? J. Neurophysiol. 68, 1558–1574 (1992). [PubMed: 1479430]
39. Martin PR & Teoh HJ. Effects of visual stimuli and a stressor on head pain. Headache 39, 705–715 (1999). [PubMed: 11279946]
40. Gray CM & Singer W. Stimulus-specific neuronal oscillations in orientation columns of cat visual cortex. Proc. Natl Acad. Sci. USA 86, 1698–1702 (1989). [PubMed: 2922407]
41. Britten KH, Shadlen MN, Newsome WT & Movshon JA. Responses of neurons in macaque MT to stochastic motion signals. Vis. Neurosci. 10, 1157–1169 (1993). [PubMed: 8257671]
42. Pesaran B et al. Investigating large-scale brain dynamics using field potential recordings: analysis and interpretation. Nat. Neurosci. 21, 903–919 (2018). [PubMed: 29942039]
43. Stern Y. Cognitive reserve in ageing and Alzheimer's disease. Lancet Neurol. 11, 1006–1012 (2012). [PubMed: 23079557]
44. Moe KE, Vitiello MV, Larsen LH & Prinz PN. Symposium: cognitive processes and sleep disturbances: sleep/wake patterns in Alzheimer's disease: relationships with cognition and function. J. Sleep Res. 4, 15–20 (1995).
45. Mander BA et al. Prefrontal atrophy, disrupted NREM slow waves and impaired hippocampal-dependent memory in aging. Nat. Neurosci. 16, 357–364 (2013). [PubMed: 23354332]
46. Lucey BP et al. Associations between β-amyloid kinetics and the β-amyloid diurnal pattern in the central nervous system. JAMA Neurol. 74, 207–215 (2017). [PubMed: 27992627]
47. Kastanenka KV et al. Frequency-dependent exacerbation of Alzheimer's disease neuropathophysiology. Sci. Rep. 9, 8964 (2019). [PubMed: 31221985]
48. Kastanenka KV et al. Optogenetic restoration of disrupted slow oscillations halts amyloid deposition and restores calcium homeostasis in an animal model of Alzheimer's disease. PLoS ONE 12, e0170275 (2017). [PubMed: 28114405]
49. Giovannetti EA et al. Restoring memory by optogenetic synchronization of hippocampus oscillations in an Alzheimer's disease mouse model. Preprint at bioRxiv 10.1101/363820 (2018).
50. Wu JW et al. Neuronal activity enhances tau propagation and tau pathology in vivo. Nat. Neurosci. 19, 1085–1092 (2016). [PubMed: 27322420]
51. Venturino A et al. Microglia enable mature perineuronal nets disassembly upon anesthetic ketamine exposure or 60-Hz light entrainment in the healthy brain. Cell Rep. 36, 109313 (2021). [PubMed: 34233180]
52. Ismail R et al. The effect of 40-Hz light therapy on amyloid load in patients with prodromal and clinical Alzheimer's disease. Int. J. Alzheimers Dis. 30, 6852303 (2018).
53. Clarke D, Crombag HS & Hall CN. An open-source pipeline for analysing changes in microglial morphology. Open Biol. 11, 210045 (2021). [PubMed: 34375551]
54. Baik SH, Kang S, Son SM & Mook-Jung I. Microglia contributes to plaque growth by cell death due to uptake of amyloid β in the brain of Alzheimer's disease mouse model. Glia 64, 2274–2290 (2016). [PubMed: 27658617]
55. Yang G, Pan F, Parkhurst CN, Grutzendler J & Gan WB. Thinned-skull cranial window technique for long-term imaging of the cortex in live mice. Nat. Protoc. 5, 201–208 (2010). [PubMed: 20134419]
56. Pachitariu M, Steinmetz N, Kadir S, Carandini M & Harris KD Fast and accurate spike sorting of high-channel count probes with KiloSort. in Advances in Neural Information Processing Systems 29 (eds Lee D et al.) (NIPS, 2016).

57. Petersen PC, Siegle JH, Steinmetz NA, Mahallati S & Buzsáki G. CellExplorer: a framework for visualizing and characterizing single neurons. Neuron. 109, 3594–3608.e2 (2021). [PubMed: 34592168]

58. Zar JH Biostatistical Analysis 4th edn (Prentice Hall, 1999).

59. Zhang Y et al. Cholinergic suppression of hippocampal sharp-wave ripples impairs working memory. Proc. Natl Acad. Sci. USA 118, e2016432118 (2021). [PubMed: 33833054]

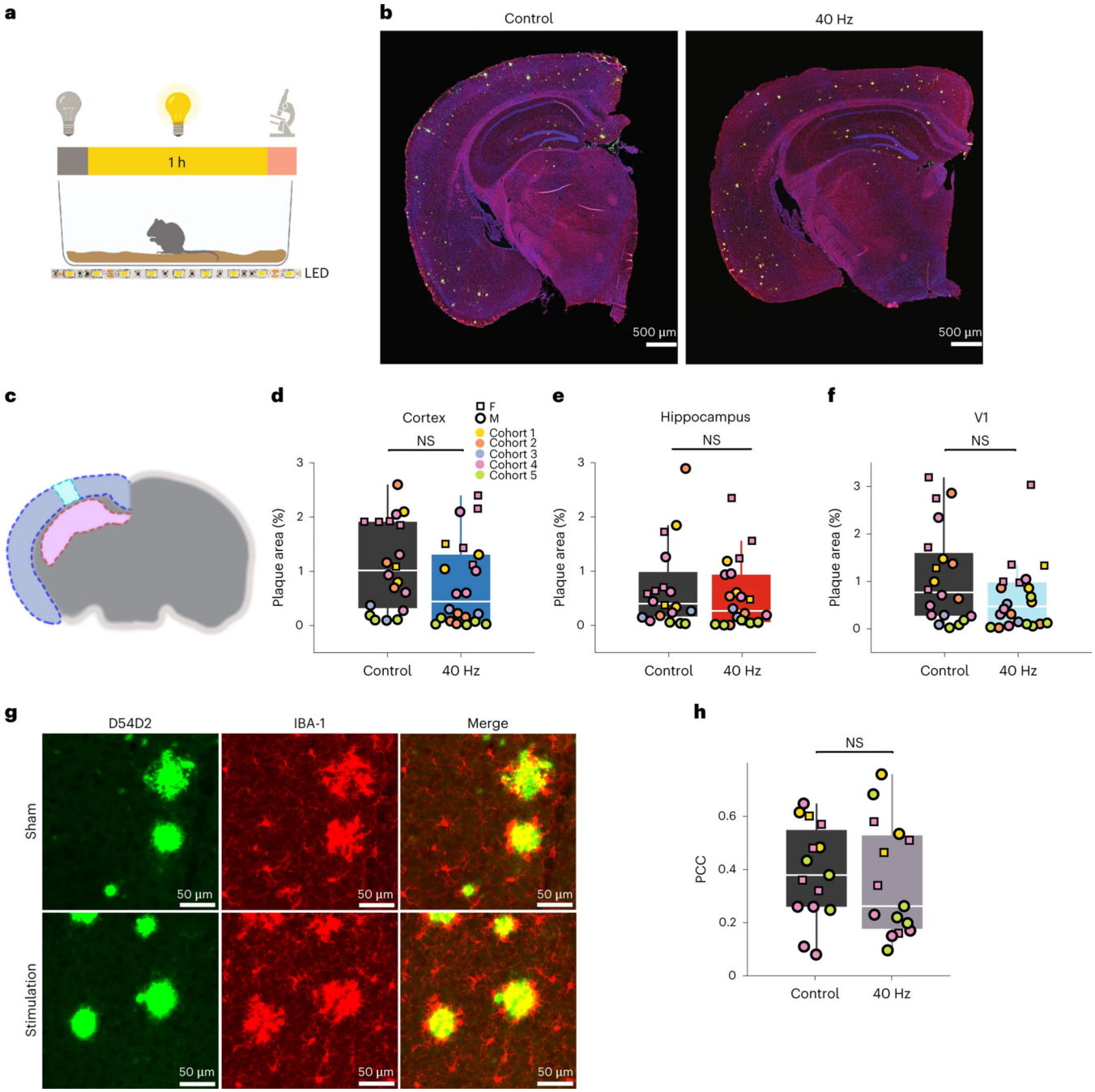

Fig. 1 |. Effect of acute 40-Hz visual simulation on Aβ load and microglia.

a, Schematic of experimental design. Baseline of 10 min followed by 1 h of control light or 40-Hz stimulation, after which the animal was killed for histological analysis. Parts created with BioRender.com. **b**, Representative IHC with superimposed anti-Aβ (D54F2, green), anti-Iba1 (microglia, red) and DAPI (blue) in two 4-month-old 5xFAD mice exposed to continuous white light (control) or 40-Hz flicker light (replicated in n = 34 mice; Supplementary Table 1). **c**, Schematic of brain areas used to quantify Aβ load in neocortex (dark blue), V1 (light blue) and hippocampus (red). **d**–**f**, Group difference

(medians, interquartile ranges, maxima and minima) of the percentage area occupied by plaques in neocortex (**d**) (NS, $P = 0.12$; two-sided Wilcoxon test), hippocampus (**e**) (NS, $P = 0.296$; two-sided Wilcoxon test) and V1 (**f**) (NS, $P = 0.15$; two-sided Wilcoxon test) (control, 20 mice; 40-Hz flicker, 22 mice). Squares are females and circles are males. The different colored dots correspond to different littermate cohorts (Extended Data Fig. 1e). **g**, High-magnification IHC pictures stained with anti-Aβ (D54D2, green) and anit-Iba1 (microglia, red) antibodies in V1 of the same two 5xFAD mice as in **b** (replicated in $n = 34$ mice for 40-Hz stimulation and $n = 31$ control mice; Supplementary Table 1). **h**, PCC between microglia and Aβ in control and 40-Hz mice (medians, interquartile ranges, maxima and minima; NS by two-sided Wilcoxon test: $P = 0.538$) (control, 15 mice; 40-Hz flicker, 15 mice). F, female; M, male; NS, not significant.

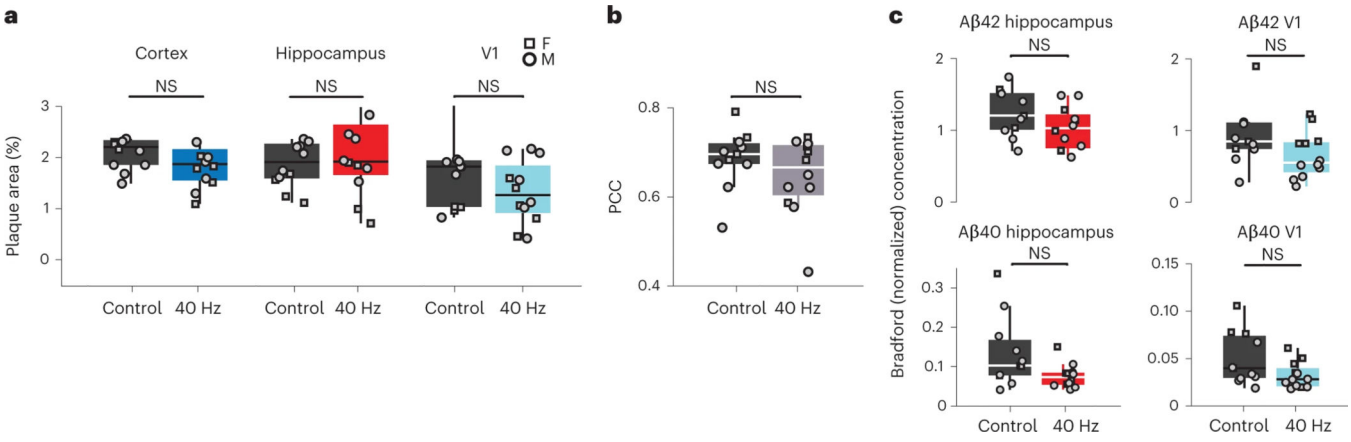

Fig. 2 |. Effect of chronic 7-d 40-Hz visual simulation.

a, Group differences (medians, interquartile ranges, maxima and minima) of the percentage area occupied by Aβ in the neocortex (NS, $P = 0.13$; two-sided Wilcoxon test), hippocampus (NS, $P = 0.479$; two-sided Wilcoxon test) and V1 (NS, $P = 0.309$; two-sided Wilcoxon test). **b**, PCC between Aβ (anti-Aβ, D54F2) and microglia (anti-Iba1, microglia) (NS, $P = 0.406$; two-sided Wilcoxon test; medians, interquartile ranges, maxima and minima). **c**, Relative human Aβ42 (hippocampus: NS, $P = 0.096$; two-sided Wilcoxon test; V1: NS, $P = 0.242$; two-sided Wilcoxon test) and Aβ40 (hippocampus: NS, $P = 0.089$; two-sided Wilcoxon test; V1: NS, $P = 0.096$; two-sided Wilcoxon test) peptide levels in hippocampus and V1 measured by ELISA and normalized to overall protein levels detected with Bradford test ($n = 11$ control; $n = 12$ 40-Hz stimulation mice; medians, interquartile ranges, maxima and minima).

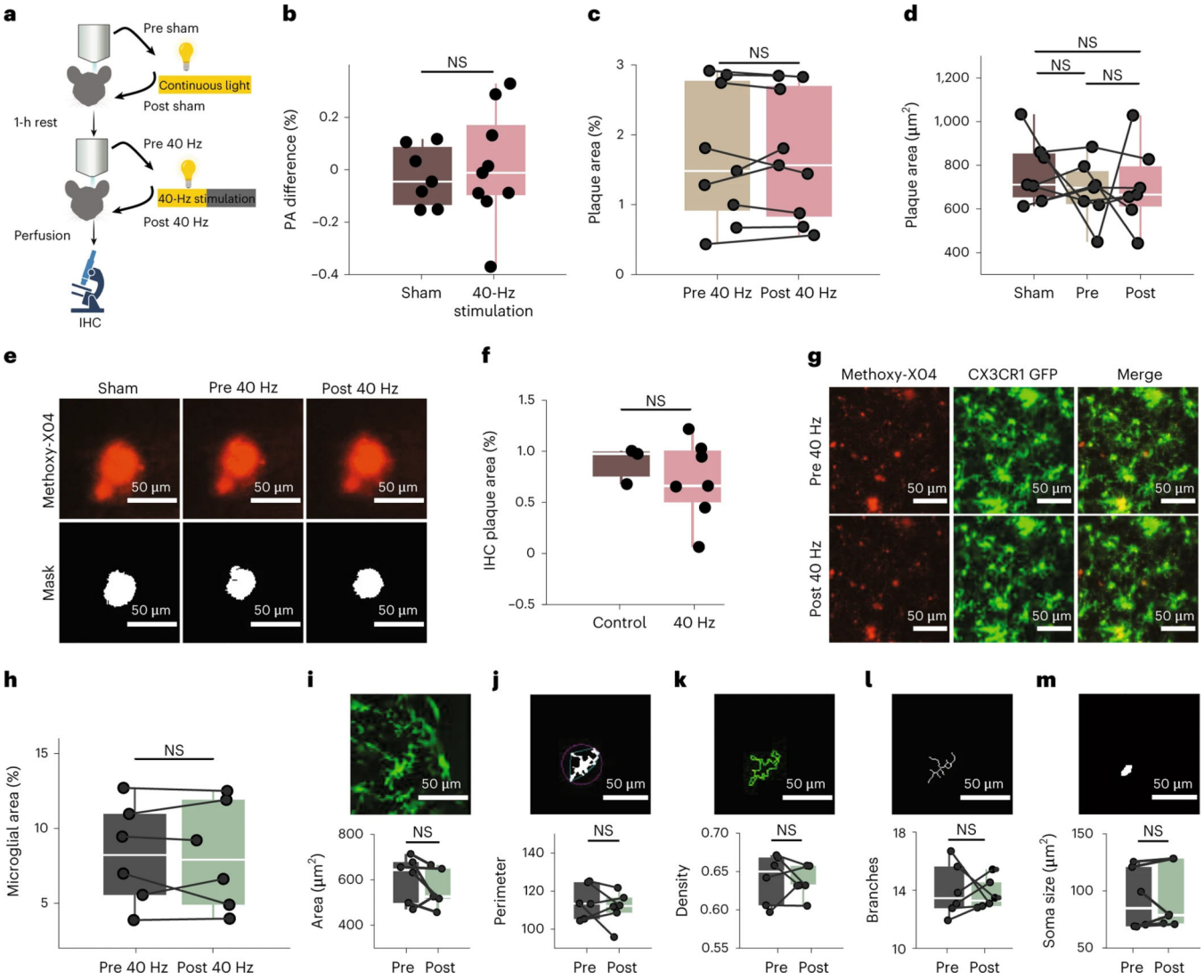

Fig. 3 |. In vivo monitoring of plaques and microglia.

a, Schematic of two-photon experiment. Mice were first imaged before and after 1 h of continuous white light stimulation, after which they were allowed to rest for 1 h in the homecage. Following rest, they were placed back in the imaging set-up and images were taken before and 1 h after 40-Hz stimulation. Parts created with BioRender.com. **b**, Differences (medians, interquartile ranges, maxima and minima) between the fractional area occupied by plaques (PA difference) in the imaged V1 before and after continuous light stimulation (sham) and before and after 40-Hz light flicker (sham, 7 mice; no stimulation, 2 mice; 40-Hz flicker, 9 mice; NS, two-sided Wilcoxon test: $P = 0.758$). **c**, Percentage plaque area (medians, interquartile ranges, maxima and minima) for the $n = 9$ mice before and after 40-Hz stimulation (NS, $P = 0.934$; two-sided Wilcoxon test). **d**, Aβ plaque area (medians, interquartile ranges, maxima and minima) did not change following 40-Hz stimulation (NS; sham–pre $P = 0.382$; pre–post $P = 0.383$; sham–post $P = 0.915$; two-sided Wilcoxon test) in $n = 7$ mice. In this comparison, individual plaques were compared before and after flicker stimulation. **e**, Example Aβ plaque image and its mask after sham stimulation,

before and after 40-Hz flicker exposure (replicated in $n = 8$ mice; Supplementary Table 2). **f**, Immunohistochemical quantification of percentage Aβ area (medians, interquartile ranges, maxima and minima) in the entire V1 in a subset of 7 mice used for two-photon experiments compared with 3 age-matched, nonstimulated control mice (NS, $P = 0.287$; two-sided Wilcoxon test). **g**, Example two-photon images of plaques. Red, methoxy-X04); green, microglia in $Cx3cr1^{GFP/+}$:$5xFAD^{+/-}$ mice and their merged version before and after 40-Hz flicker stimulation (replicated in $n = 6$ mice; Supplementary Table 2). **h**, Percentage occupancy of microglia (medians, interquartile ranges, maxima and minima) in the imaged area before and after 40-Hz flicker stimulation (bottom; $n = 6$ mice; NS, $P = 0.932$; two-sided Wilcoxon test). **i**–**m**, Further morphological analyses for microglial parameters (ref. [53]) (medians, interquartile ranges, maxima and minima). **i**, Glial area, quantified as the total number of pixels present in the filled shape (μm^2; NS, $P = 0.484$; two-sided Wilcoxon test). **j**, Cell perimeter (the number of pixels in μm that outline the cell; NS, $P = 0.589$; Wilcoxon test). **k**, Density = area/convex hull area (NS, $P = 0.484$; two-sided Wilcoxon test). **l**, Number of branches in each microglia (NS, $P = 0.766$; two-sided Wilcoxon test). **m**, The soma size (the pixel area μm^2 occupied by the microglial soma mask; NS, $P = 0.793$; two-sided Wilcoxon test).

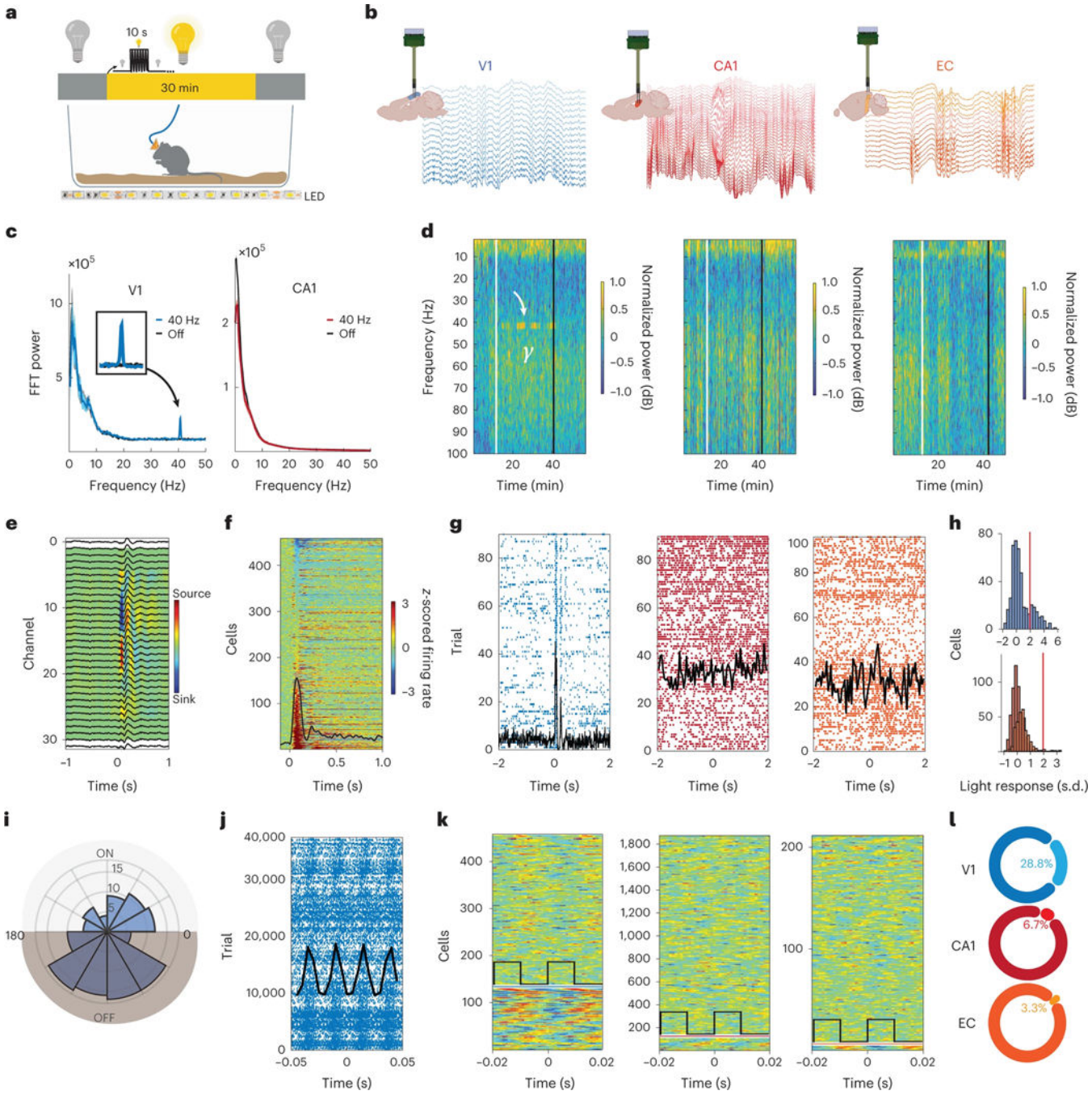

Fig. 4 |. A 40-Hz visual simulation does not engage native gamma oscillations.

a, Schematic of the experimental design. Headgear is shielded by a 3D-printed copper mesh cap. Baseline of 10 min followed by 30 min of 40-Hz stimulation (10 s on, 10 s off) and 10 min of control recording. Parts created with BioRender.com. **b**, Mice were implanted with silicon probes in V1, CA1 or EC. Example LFP depth profiles for each brain region. **c**, Mean power spectra ± s.e.m. from V1 (blue) and hippocampal CA1 (red) recording sites during interleaved 40-Hz stimulation and no-stimulation epochs, overlayed. Narrow-band 40-Hz response is only seen in V1 during light stimulation (inset shows enlarged part of 40-Hz

response). **d**, Example time-resolved spectrogram of V1, CA1 and EC recordings. White and black vertical lines mark the onset and offset of 40-Hz stimulation, respectively. Curved arrow, narrow-band, 40-Hz (γ) in V1. Note intermittent, brain-state-dependent responses despite continuous 40-Hz stimulation. **e**, Example average LFP traces (black) and current source density map in V1, triggered by the onset of 40-Hz trains every 10 s. The color scale indicates current density (a.u.). **f**, *z*-scored single neuron responses in V1 ($n = 458$ neurons in 5 mice) to the onset of 40-Hz trains every 10 s. Overlayed in black is the average response signal. **g**, Example peristimulus time histograms of example neurons in V1 (blue), CA1 (red) and EC (orange). Black, average firing rate. **h**, Distribution of *z*-scored light responses. Note low fraction of significantly responding neurons (red line, *z*-score > 1.96) in CA1 (red) and EC (orange). **i**, Phase distribution of significantly phase-modulated V1 neurons. **j**, Example of same V1 cell (**g**) peristimulus time histogram around 40-Hz stimulus. **k**, *Z*-scored single neuron responses in V1 ($n = 458$ neurons in 5 mice), CA1 ($n = 1,874$ neurons in 15 mice) and EC ($n = 211$ neurons in 3 mice) to 40-Hz stimulation. The horizontal line separates nonmodulated cells (above) from modulated neurons (below). **l**, Percentage of 40-Hz-modulated cells in V1 (blue), CA1 (red) and EC (orange). FFT, Fast Fourier transforms.

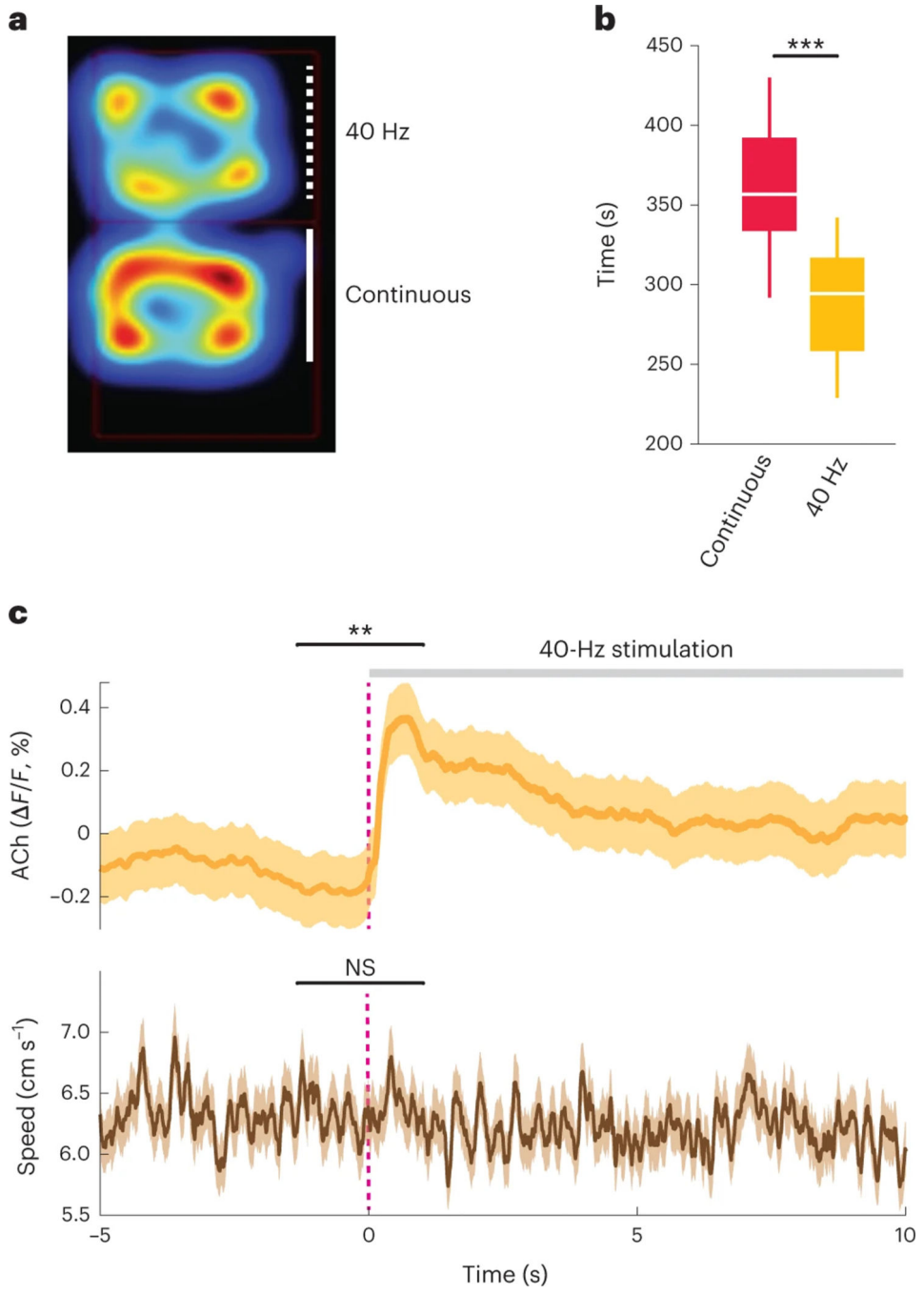

Fig. 5 |. A 40-Hz flickering stimulation is aversive.

a, Example of a mouse's movement trajectory in a two-compartment (40-Hz flickering light and continuous light, respectively) apparatus. **b**, Group average time spent in the respective compartments ($n = 14$ mice; $^{***}P = 3.59 \times 10^{-4}$, two-sided Wilcoxon test). **c**, Ach3.0 fluorescence signal, measured by GRAB fiber photometry ($^{**}P = 0.0014$, two-tailed paired *t*-test) and movement (NS, $P = 0.67$, two-tailed paired *t*-test) recorded during alternating 10 s on, 10 s off 40-Hz light stimulation (40 min).